Interface magnetism of 3d transition metals

Niklasson, A. M. N.; Johansson, B.; Skriver, Hans Lomholt

Published in:
Physical Review B

Link to article, DOI:
10.1103/PhysRevB.59.6373

Publication date:
1999

Document Version
Publisher's PDF, also known as Version of record

Interface magnetism of 3*d* transition metals

A. M. N. Niklasson and B. Johansson
Condensed Matter Theory Group, Physics Department, Uppsala University, S-75121 Uppsala, Sweden

H. L. Skriver
Center for Atomic-scale Materials Physics and Department of Physics, Technical University of Denmark, DK-2800 Lyngby, Denmark

(Received 22 July 1998)

The layered resolved magnetic spin moments of the magnetic 3*d* bilayer interfaces Fe/V bcc, Fe/Co bcc, Fe/Cu bcc, Co/V bcc, Co/Ni fcc, Co/Cu fcc, Ni/V fcc, Ni/Cr fcc, Ni/Cu fcc and the magnetic surfaces Fe bcc, Co bcc, Co fcc, and Ni fcc are calculated for the (001), (011), and (111) orientations by means of a first-principles Green's function method. It is shown how the magnetic profiles around the bilayer interfaces and surfaces directly can be used to predict the magnetization of more complex systems such as magnetic multilayers and clusters. Furthermore, it is shown how the magnetic interface moments can be estimated from data of the corresponding binary bulk alloys. The behavior of interface magnetism can thus be traced back to the understanding of magnetism in bulk alloys. [S0163-1829(99)04005-9]

I. INTRODUCTION

Fascinating possibilities within materials science are connected to magnetic multilayers, e.g., metallic sandwiches with a varying number of magnetic/nonmagnetic layers. These systems offer the possibility of designing new materials with unique tailor-made magnetic properties. In order to achieve this in an efficient way we need to be able to predict the magnetization in these layered systems. One important part of the magnetization in multilayers is determined by the long-ranged, but weak, oscillatory magnetic interlayer coupling[1–3] that determines the mutual relation between the magnetic moments of different magnetic layers separated by paramagnetic spacers. A lot of work has been devoted to this subject, partly due to the technological possibilities provided by these new materials. However, for a single magnetic bilayer interface between a ferromagnetic and a paramagnetic crystal the magnetization is determined by the mutual perturbation between the two materials in the interface region. Less work has been done on this more short-ranged part of the magnetic ordering that may give rise to an enhanced or decreased interface magnetism as well as to an oscillatory shape of the magnetization profile in the interface region. It is this kind of interface magnetism that will be addressed in the present work. First we investigate the layered resolved magnetic profiles for a number of different metallic bilayer interfaces. We also explain how the magnetic interface moments can be understood in terms of the corresponding binary bulk alloys. Thereafter we show how the magnetic interface profiles directly can be used, by means of superposition, to estimate the magnetization of more complex layered systems. To include surface overlayers also, magnetic profiles of surfaces have been calculated. With this technique of superimposing magnetization profiles of independent bilayers and surfaces we have obtained an efficient way to predict the magnetic profiles of a variety of layered magnetic structures. However, the technique is not limited only to layered systems. With the same technique it is also possible to estimate the magnetization of almost any kind of object demarcated by planar interfaces, for example, free and embedded atomic clusters. A similar kind of superposition has, for example, been shown to be useful in order to investigate the environmental effects on the hyperfine field in Ni_xFe_{1-x} alloys.[4]

In the present work spin-density-functional theory has been used in order to calculate the magnetic profiles of interfaces between the 3*d* transition metals as well as the magnetic profiles of Fe, Co, and Ni surfaces. Some of the metals in the 3*d* series have very complex magnetic structures or are very sensitive to changes in the lattice constant such as Mn, Cr bcc, Ni bcc, and Fe fcc. Interfaces with these materials will therefore not be considered in the present study where only the magnetic profiles of interfaces between bcc V, Co, Fe, Cu and fcc V, Cr, Co, Ni, Cu, and surfaces of bcc Fe, bcc/fcc Co, and fcc Ni will be investigated.

In Sec. II we explain the calculational method and in Sec. III we discuss the magnetic profiles of the bilayer interfaces and surfaces. In Sec. IV it is shown how the magnetic interface moments can be connected to the magnetic moment of the corresponding binary alloys and in Sec. V we show how the magnetization profiles directly can be used to estimate the magnetization of trilayers and multilayers. In Sec. VI this technique is generalized to include also nonlayered systems such as free and embedded clusters.

II. CALCULATIONAL DETAILS

The magnetic spin moments in the present study have been calculated self-consistently within the framework of density-functional theory[5,6] in its local spin-density approximation.[7,8] The calculational method is based on the linear-muffin-tin-orbital method[9–12] (LMTO) and the corresponding Green's function technique for surfaces and interfaces as developed by Skriver and Rosengaard.[13] The method exploits the short-range nature of the structure constants, i.e., the short range of the overlap between the LMTO

basis functions in the tight-binding representation, to construct thin so-called principal layers, of a few atomic monolayers thickness, with vanishing overlap between next-nearest principal layers. The principal layers can be glued together or cut apart by means of Löwdin downfolding[14] in such a way that only successive operators of limited sizes have to be inverted to construct the Green's function of the entire system. With this so-called principal-layer technique[15,16] the total amount of work scales linearly with the number of nonequivalent atoms, which is of major importance for the study of large extended systems. The Green's function technique does not rely on a slab or supercell geometry and therefore ensures a correct description of the broken translational symmetry perpendicular to the interface. The method is especially well suited for closed-packed systems since the atomic-sphere approximation is used.

The bilayer interface systems investigated in the present study consist of two semi-infinite crystals A and B that are put together to form an A/B interface. Far away from the interface the magnetic moment will be equal to the moment of the corresponding bulk material that may be magnetic or nonmagnetic. The width of the region for charge and spin relaxation was chosen to be nine or ten monolayers on each side of the interface. The surfaces are treated by means of the same technique, where one of the semi-infinite crystals is replaced by empty spheres. Also the trilayer systems, which consist of some spacer material X embedded between two semi-infinite crystals A and B, i.e., $A/X/B$, are treated in the same way. The number of special k points[17] in the irreducible part of the two-dimensional Brillouin zone was chosen to be 36, 64, and 90 for the (001), (011), and (111) interfaces, respectively. All interface calculations were done for a fixed lattice around the interfaces, i.e., no relaxations were taken into account. The symmetry is broken only in the direction perpendicular to the interfaces and all atoms are considered to be equal within each individual atomic layer. Since an interface usually is formed either by growing material A on top of B or *vice versa* the lattice constant was determined by the atomic volume of the experimental ground-state structure of either material A or material B. Differences between the magnetic profiles for these two volumes give an estimate of relaxation effects. Since volume-conserving tetragonal distortions usually only have a small influence on the magnetic spin moment,[18] one can expect that the magnetic moment of material A for a volume appropriate for A and material B for a volume appropriate B will be most correct.

III. MAGNETIC BILAYERS AND SURFACES

In Figs. 1(a)–1(i) we display the magnetic profiles of interfaces between bcc structures for V, Co, Fe, Cu and fcc structures for V, Cr, Co, Ni, Cu in the (001), (011), and (111) orientations. The calculated numerical values of the layered resolved moments are tabulated in Table I. All interfaces are chosen to consist of at least one magnetic material. The magnetic profiles are shown for the two lattice constants of the two interface materials. The lattice constant is indicated by the corresponding bulk material within the parentheses for each profile, i.e., ''fcc (011) (A)'' means an A/B fcc (011) interface calculated at the lattice constant determined by the experimental equilibrium volume of material A. Deviations between the magnetic profiles for these two lattice volumes give an estimate of relaxation effects on the magnetization. In the figures no dramatic volume effects are seen except for the Co/V bcc (111) interface where the spin moment of the Co interface layer is increased by a factor of 3 when the lattice constant is increased by about 7% when going from the lattice constant of Co to that of V. However, the shape of the magnetic profile of the interface is not drastically changed. It is interesting to note that in the case of Co/V bcc (111) the magnetic moment of the interface layer has a much stronger volume dependence than further away from the interface. This highly increased magnetovolume sensitivity at an interface is not seen for other interfaces in the present study.

The small rather long-ranged oscillations that are found in the magnetic profiles can be looked upon as magnetic Friedel oscillations due to spin-dependent screening of the perturbation caused by the presence of the neighboring layer material at the interfaces.

The interfaces with V and Cr deviate slightly from the other interfaces since these two materials induce a rapid decay of the magnetic moments of the outermost neighboring magnetic interface layer. The explanation for the different trends of the interface magnetization will be given below where we investigate the relation between the magnetization of the interfaces and the corresponding bulk alloys.

In Table II the layer-resolved spin moments of surfaces of Fe bcc, Co bcc, Ni fcc, and Co fcc are shown for the (001), (011), and (111) orientations. Some of the surface magnetization profiles, calculated with the same method, have been published elsewhere[19] and compared with other calculations.[20–25] Looking at the table we find, with the exception of the Ni fcc (111) surface, a small enhancement of the magnetic moment of the outermost surface layer. The enhancement can be explained as an effect due to the reduced coordination of the surface layer that leads to a more narrow layer-projected surface density of states. This generally increases the number of states around the Fermi level, a circumstance that favors a higher magnetic moment at the surface. Especially we notice the increased magnetic moments for the more open surfaces, i.e., bcc (111) and fcc (011), whereas the more closed-packed surfaces such as bcc (011) and fcc (111) have slightly less enhanced magnetic surface moments. A somewhat similar trend is seen also in case of the magnetic bilayers where the more closed interfaces are perturbed less and the magnetic interface moments are therefore more close to the corresponding bulk values. However, in contrast to the magnetic surfaces, we do not always find an increased magnetic interface moment compared to bulk for the more open interfaces.

IV. RELATION TO BULK ALLOYS

Layered resolved magnetic interface moments are hard to determine experimentally. A few measurements have been done by means of the element specific magnetic circular x-ray dichroism for atoms in ultrathin overlayers,[26,27] which may give information on the interface magnetism of buried layers. Also measurements of the total magnetization of layered systems can be used in order to estimate magnetic ef-

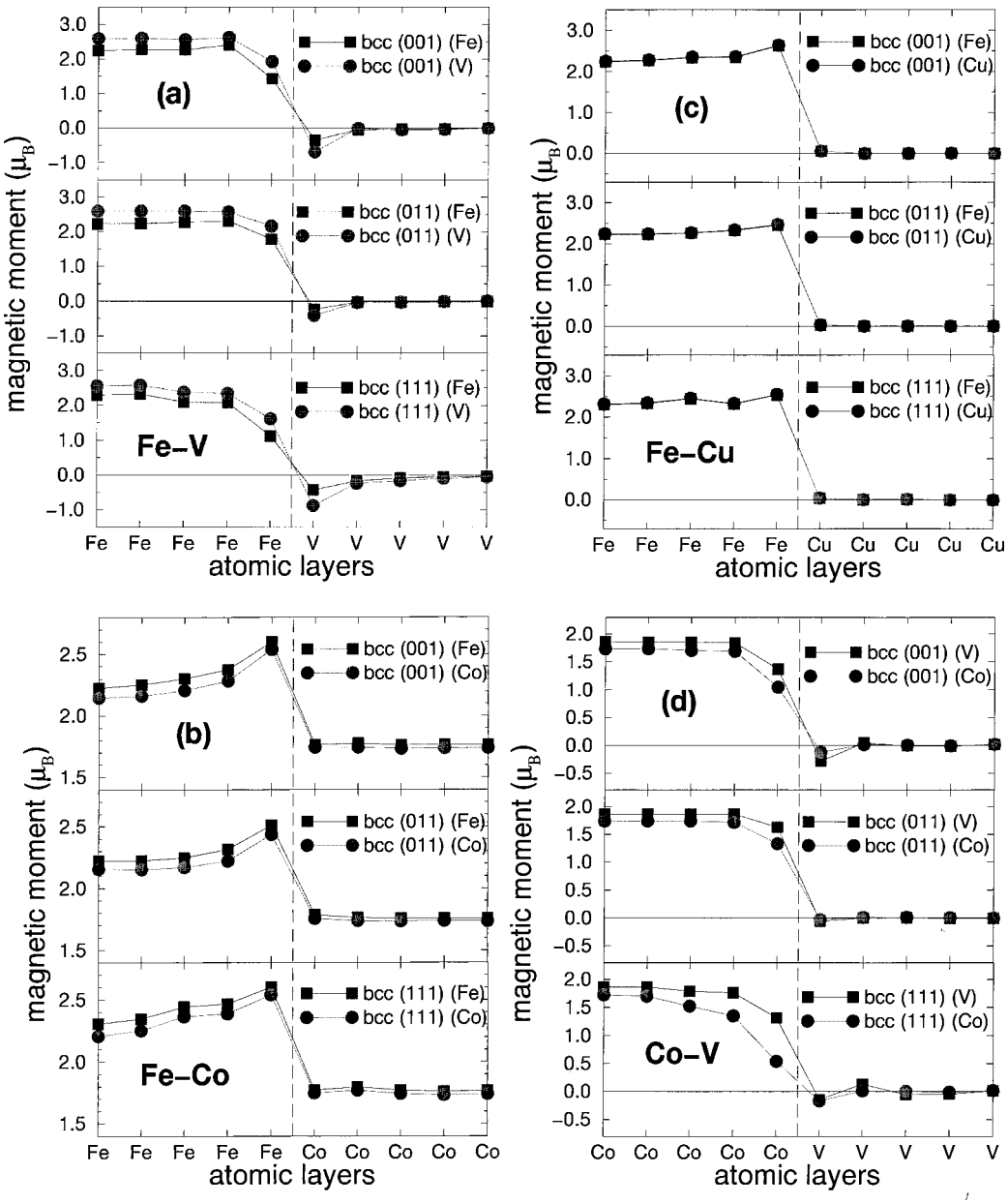

FIG. 1. The calculated profiles of the layer-projected magnetic spin moments of different magnetic bilayer interfaces are shown in (a)–(i). The lattice constant is indicated by the corresponding bulk material within the parentheses in each figure.

fects of the interfaces. Recently some attempts have been made to extract layer-resolved magnetic moments from measurements of the hyperfine fields near metallic interfaces,[28,29] but roughness, diffusion, and questions concerning the relation between the hyperfine field and the magnetic moment close to an interface make it difficult to derive such information. However, a large amount of data can be found for the corresponding binary bulk alloys between the constituent interface materials. If it is possible to establish a relation between the magnetic moment of the binary bulk alloy and the interface moments we may use available data for alloys to estimate the interface magnetization.

An outermost interface atom A of an A/B interface is in its nearest-neighboring shell surrounded by n_A number of A atoms and n_B number of B atoms. We now define an averaged interface moment $m_{AB}^{\mathrm{IF}}(x)$ as

$$m_{AB}^{\mathrm{IF}}(x) = x m_A^{\mathrm{IF}} + (1-x) m_B^{\mathrm{IF}}, \tag{1}$$

where $x = n_A/(n_A+n_B)$ and m_A^{IF} and m_B^{IF} are the magnetic moments of the outermost A and B interface atoms, respectively. This averaged interface moment can be interpreted as the magnetic moment of a highly correlated (ordered) bulk alloy if we neglect the fact that the outermost B atom at the interface actually has n_A number of B atoms in its nearest-neighboring shell. Thus, if more long-range ordering effects on the individual magnetic moments in the alloy are small, there should be a good agreement between the averaged interface moment and the magnetization of the corresponding bulk alloys. In Fig. 2 we have plotted the averaged interface magnetization $m_{AB}^{\mathrm{IF}}(x)$ for the interfaces as a function of the average valence charge $\overline{N} = x N_A + (1-x) N_B$, where N_A and

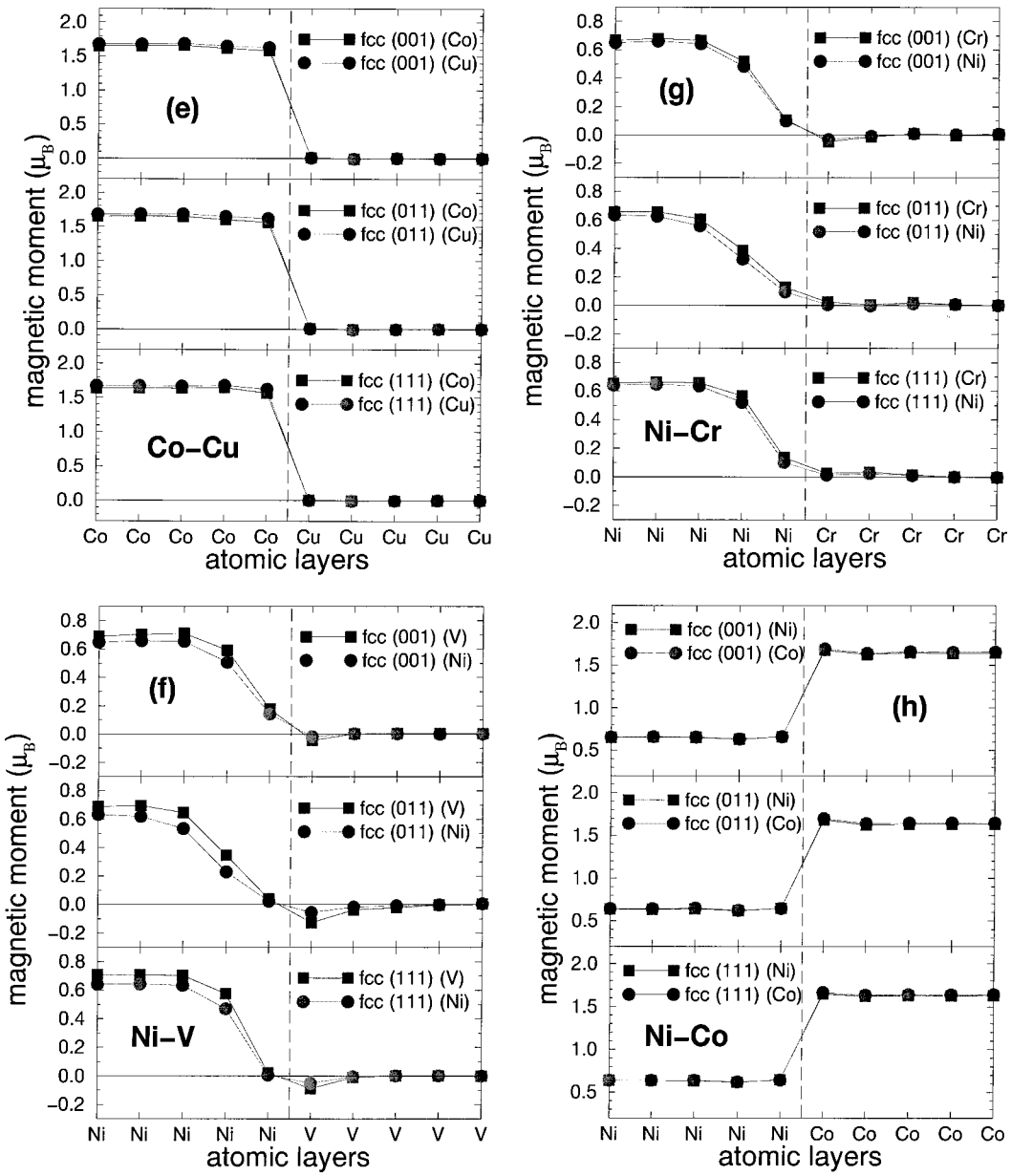

FIG. 1. (*Continued.*)

N_B are the number of valence electrons of the constituent materials, i.e., a kind of Slater-Pauling graph for the interface magnetization.

The similarity between this graph and the well-known Slater-Pauling curve for the 3*d* alloys clearly elucidate the relation between the magnetic interface moments and the corresponding bulk alloys. The dashed lines display some of the experimental data for the magnetic moments for bulk alloys.[30] If the magnetic moment of the individual atomic types does not change in the alloy or at the interface as a function of mixing concentration, or interface orientation, the magnetization curves in the Slater-Pauling graph will be straight lines between the magnetic moments of the constituent pure bulk materials. Deviations from such a linear interpolation therefore indicate changes of the magnetic moments compared to the bulk for the individual atomic types in the alloy and at the interface. For example, the increased interface moment of Fe at the Fe/Co interfaces can be explained in terms of the increased total magnetization of the Fe_xCo_{1-x} alloy for small concentrations of Co in Fe. This increase is mainly due to an increased Fe moment since the Co moment is saturated, in full agreement with what is found at the interface. Furthermore, the linear behavior of the magnetization curve between Co and Ni for the experimental Co_xNi_{1-x} alloy indicates that there is no large deviation of the interface magnetization in the Co/Ni interface compared to bulk Co and Ni, which is in complete agreement with the calculated magnetic interface moments. In the same way we can understand, for example, the decreased magnetic interface moments of Ni at the Ni/V, Ni/Cr, and Ni/Cu interfaces. Thus, deviations from a linear behavior of the Slater-Pauling curve between two materials for a binary bulk alloy indicate that the corresponding interface moments are different from bulk. If the Slater-Pauling curve is below the linear interpolation at least one of the interface moments is less than in bulk and opposite if it is higher. A more quantitative estimate of the

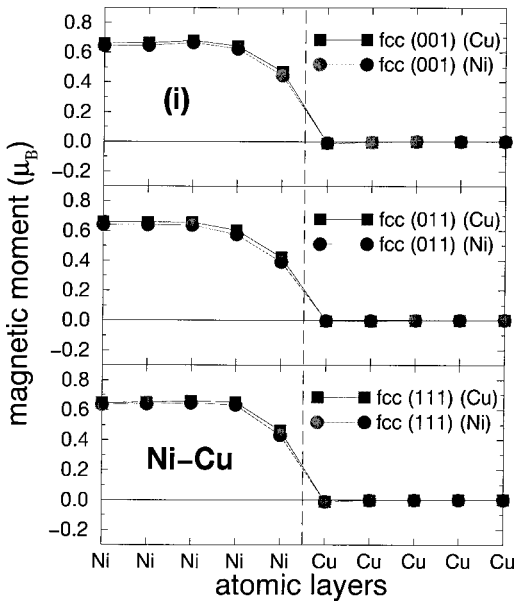

FIG. 1. (*Continued.*)

magnetic interface moments might be achieved if the atomic projected magnetic moments $m_A(x)$ and $m_B(1-x)$ of an A_xB_{1-x} alloy are known through the relations

$$m_A^{\mathrm{IF}} \approx m_A(x), \quad m_B^{\mathrm{IF}} \approx m_B(1-x), \tag{2}$$

where $x=n_A/(n_A+n_B)$ and n_A, n_B are the number of A and B atoms in the first coordination shell around an outermost A interface atom. The reason for this is that we now compare atomic projected moments in the bulk alloy and at the interface with the same number of nearest neighbors and one can expect that this leads to a better quantitative estimate of the magnetic interface moments. Recently, in a systematic theoretical study of binary bulk alloys between Fe, Co, Ni, and Cu,[31] it was shown that more long-ranged correlation effects usually only have a small effect on the magnetization. This supports the possibility of a quantitative comparison between the magnetization of a disordered bulk alloy and the magnetic moments at an interface. The explanation of the behavior of the interface magnetism can thus be traced back to the understanding of magnetism in bulk alloys.

V. MAGNETIC TRILAYERS

In this section we show how the magnetic profile of trilayer systems can be approximated by superpositions of the magnetic profiles of free-standing bilayer interfaces if multiple-scattering effects such as quantum-well states[32–34] are neglected. The method can be naturally extended to be valid also for magnetic multilayers and surface overlayers. In this way the magnetic interface and surface profiles of the previous section, Table I, and Table II, can be used to analyze more complex layered magnetic structures. The discussion is close to previous work[35] where it was shown how multiple-scattering effects such as quantum-well states only give a small, almost constant, contribution to the magnetic profile in Fe/Cu/Fe trilayers. Multiple-scattering effects can sometimes be important for the magnetization in thin films and may even induce an onset of magnetism in paramagnetic materials[36] or quench the magnetism in ferromagnetic materials.[37] However, these enhancements or quenching effects are mainly of importance for thin films of nearly magnetic materials such as Rh, Pd, and Pt. Thus, except multiple scattering, also certain enhancement/quenching effects are neglected in the following discussion, but as will be shown, this has only a small effect on the magnetization profile.

A trilayer system consists of two semi-infinite crystals separated by a number of atomic monolayers of some spacer material. The semi-infinite crystals on the left- (L) and right-hand (R) sides of the trilayer may be regarded as spin-dependent perturbations V_L^σ and V_R^σ, which create a magnetic quantum well (QW) surrounding the spacer material. Notice that also a nonmagnetic material creates a magnetic perturbation on a magnetic material. One of the semi-infinite crystals may be vacuum, i.e., the trilayer case in the present discussion also includes the case of surface overlayers. The magnetic perturbations change the ground-state Green's function G_0^σ of the bulk spacer material and the perturbed Green's function G^σ may be obtained from a Dyson series that can be separated as follows:

$$G^\sigma = G_0^\sigma + \Delta G_L^\sigma + \Delta G_R^\sigma + \Delta G_{QW}^\sigma. \tag{3}$$

Here σ denotes the separate spin channels and

$$\Delta G_L^\sigma = G_0^\sigma V_L^\sigma G_0^\sigma + G_0^\sigma V_L^\sigma G_0^\sigma V_L^\sigma G_0^\sigma + \cdots, \tag{4}$$

$$\Delta G_R^\sigma = G_0^\sigma V_R^\sigma G_0^\sigma + G_0^\sigma V_R^\sigma G_0^\sigma V_R^\sigma G_0^\sigma + \cdots, \tag{5}$$

and

$$\Delta G_{QW}^\sigma = G_0^\sigma V_L^\sigma G_0^\sigma V_R^\sigma G_0^\sigma + \cdots. \tag{6}$$

In these equations $\Delta G_{L(R)}^\sigma$ includes all scattering events at the left(right)-hand potential barrier that may be recognized as a single-interface perturbation of the spacer material due to the magnetic semi-infinite crystal on the left(right), without any interaction with the semi-infinite crystal on the opposite side. This will give rise to a magnetic profile on the left(right) hand side:

$$m_{L(R)}(r) = -\frac{1}{\pi}\int^{E_F} dE\ \mathrm{Im}[G_0^\uparrow(r,r,E) + \Delta G_{L(R)}^\uparrow(r,r,E) - G_0^\downarrow(r,r,E) - \Delta G_{L(R)}^\downarrow(r,r,E)], \tag{7}$$

which we can identify as the magnetic profile of a freestanding bilayer interface. The mixed interaction term ΔG_{QW}^σ includes all multiple-scattering events in the quantum well (QW) related to the presence of both interfaces. This multiple scattering may give rise to, for example, quantum-well states similar to standing waves in a box.

From Eq. (3) one may define a Green's function

$$\tilde{G}^\sigma = G_0 + \Delta G_L^\sigma + \Delta G_R^\sigma, \tag{8}$$

which does not include the multiple-scattering contributions. The magnetic profile corresponding to this Green's function is

TABLE I. The layer-resolved magnetic spin moments in units of Bohr magnetons of the $3d$ interfaces. The lattice constant is given by the experimental equilibrium volume of the constituent interface materials and is given within parentheses.

	$I-5$	$I-4$	$I-3$	$I-2$	$I-1$	$I-0$	$I+0$	$I+1$	$I+2$	$I+3$	$I+4$	$I+5$
Fe/V bcc												
(100) (Fe)	2.230	2.244	2.269	2.260	2.411	1.434	−0.352	−0.044	−0.035	−0.027	−0.005	−0.003
(100) (V)	2.602	2.588	2.597	2.560	2.623	1.929	−0.688	−0.011	−0.052	−0.036	−0.008	−0.003
(110) (Fe)	2.224	2.226	2.235	2.277	2.307	1.788	−0.240	−0.034	−0.028	−0.024	−0.012	−0.001
(110) (V)	2.600	2.596	2.593	2.595	2.569	2.162	−0.414	−0.038	−0.036	−0.011	0.001	0.003
(111) (Fe)	2.328	2.298	2.324	2.090	2.079	1.115	−0.431	−0.167	−0.083	−0.050	−0.032	−0.033
(111) (V)	2.606	2.551	2.581	2.379	2.340	1.614	−0.876	−0.236	−0.159	−0.090	−0.048	−0.050
Fe/Co bcc												
(100) (Fe)	2.227	2.226	2.253	2.302	2.376	2.600	1.766	1.776	1.763	1.764	1.766	1.762
(100) (Co)	2.156	2.145	2.161	2.204	2.283	2.540	1.743	1.744	1.733	1.736	1.738	1.734
(110) (Fe)	2.230	2.222	2.225	2.248	2.316	2.511	1.784	1.764	1.758	1.758	1.756	1.758
(110) (Co)	2.166	2.155	2.152	2.169	2.220	2.436	1.756	1.738	1.736	1.738	1.735	1.734
(111) (Fe)	2.267	2.307	2.344	2.441	2.466	2.601	1.774	1.797	1.773	1.763	1.769	1.769
(111) (Co)	2.168	2.206	2.250	2.363	2.388	2.540	1.748	1.769	1.743	1.733	1.741	1.740
Fe/Cu bcc												
(100) (Fe)	2.240	2.229	2.259	2.332	2.343	2.622	0.059	−0.001	−0.004	0.002	−0.001	0.000
(100) (Cu)	2.253	2.244	2.278	2.348	2.359	2.636	0.059	−0.002	−0.004	0.002	−0.002	0.000
(110) (Fe)	2.229	2.227	2.230	2.256	2.322	2.456	0.028	−0.004	0.001	0.002	−0.000	0.000
(110) (Cu)	2.241	2.241	2.242	2.270	2.336	2.472	0.028	−0.004	0.001	0.002	−0.001	0.000
(111) (Fe)	2.256	2.299	2.330	2.444	2.317	2.539	0.042	0.004	0.010	−0.002	−0.005	0.002
(111) (Cu)	2.276	2.317	2.347	2.458	2.332	2.553	0.041	0.004	0.010	−0.002	−0.005	0.002
Co/V bcc												
(100) (Co)	1.735	1.737	1.732	1.707	1.689	1.044	−0.124	0.013	0.001	−0.007	0.012	0.001
(100) (V)	1.850	1.859	1.853	1.853	1.847	1.370	−0.288	0.045	−0.008	−0.012	0.017	0.006
(110) (Co)	1.736	1.737	1.739	1.735	1.716	1.331	−0.032	0.013	0.010	0.005	0.003	0.000
(110) (V)	1.859	1.858	1.863	1.857	1.866	1.628	−0.059	−0.002	0.005	−0.003	−0.005	−0.006
(111) (Co)	1.752	1.730	1.702	1.528	1.348	0.543	−0.165	0.016	0.006	−0.009	0.018	−0.008
(111) (V)	1.860	1.868	1.868	1.792	1.760	1.319	−0.144	0.136	−0.054	−0.046	0.013	−0.040
Co/Cu fcc												
(100) (Co)	1.652	1.654	1.649	1.661	1.616	1.584	0.011	−0.006	0.001	−0.001	0.000	−0.001
(100) (Cu)	1.678	1.683	1.679	1.688	1.653	1.634	0.006	−0.007	0.001	−0.001	−0.000	−0.001
(110) (Co)	1.639	1.648	1.651	1.650	1.603	1.565	0.008	−0.007	−0.006	−0.002	−0.001	0.001
(110) (Cu)	1.676	1.682	1.685	1.687	1.648	1.620	0.003	−0.008	−0.006	−0.003	−0.001	0.001
(111) (Co)	1.640	1.638	1.640	1.635	1.645	1.566	0.004	−0.005	−0.001	−0.000	−0.000	−0.002
(111) (Cu)	1.674	1.674	1.674	1.669	1.678	1.622	0.000	−0.006	−0.002	0.001	0.001	−0.001
Ni/V fcc												
(100) (Ni)	0.647	0.647	0.660	0.654	0.505	0.140	−0.018	0.002	0.001	0.000	0.000	0.001
(100) (V)	0.690	0.690	0.703	0.710	0.592	0.176	−0.045	0.003	0.005	0.005	0.004	0.004
(110) (Ni)	0.643	0.633	0.620	0.533	0.230	0.023	−0.056	−0.018	−0.008	−0.001	0.005	0.001
(110) (V)	0.702	0.688	0.696	0.646	0.345	0.038	−0.126	−0.038	−0.023	−0.003	0.005	0.002
(111) (Ni)	0.634	0.641	0.643	0.635	0.471	0.007	−0.051	−0.006	0.002	0.001	0.000	0.000
(111) (V)	0.702	0.707	0.708	0.702	0.575	0.022	−0.089	−0.010	0.001	0.001	0.000	−0.003
Ni/Cr fcc												
(100) (Ni)	0.647	0.649	0.661	0.642	0.484	0.099	−0.032	−0.010	0.009	0.002	0.006	0.005
(100) (Cr)	0.665	0.667	0.680	0.666	0.518	0.107	−0.047	−0.015	0.008	−0.003	0.002	0.004
(110) (Ni)	0.641	0.634	0.626	0.560	0.325	0.094	0.005	−0.004	0.012	0.007	−0.000	−0.001
(110) (Cr)	0.664	0.656	0.656	0.608	0.388	0.129	0.023	0.004	0.021	0.008	0.000	−0.001
(111) (Ni)	0.636	0.640	0.646	0.636	0.521	0.103	0.012	0.024	0.010	0.000	−0.003	0.002
(111) (Cr)	0.651	0.654	0.662	0.658	0.566	0.136	0.025	0.034	0.015	0.000	−0.005	0.005

TABLE I. (*Continued.*)

	$I-5$	$I-4$	$I-3$	$I-2$	$I-1$	$I-0$	$I+0$	$I+1$	$I+2$	$I+3$	$I+4$	$I+5$
Ni/Co fcc												
(100) (Ni)	0.648	0.649	0.654	0.650	0.628	0.658	1.677	1.628	1.647	1.639	1.643	1.640
(100) (Co)	0.652	0.653	0.659	0.654	0.631	0.660	1.692	1.641	1.659	1.651	1.655	1.652
(110) (Ni)	0.638	0.636	0.634	0.642	0.619	0.644	1.683	1.623	1.633	1.631	1.632	1.629
(110) (Co)	0.644	0.642	0.640	0.648	0.622	0.646	1.700	1.640	1.648	1.646	1.646	1.644
(111) (Ni)	0.635	0.638	0.638	0.635	0.618	0.645	1.648	1.623	1.631	1.626	1.630	1.626
(111) (Co)	0.638	0.641	0.641	0.638	0.620	0.644	1.661	1.634	1.641	1.636	1.640	1.636
Ni/Cu fcc												
(100) (Ni)	0.652	0.646	0.648	0.665	0.623	0.442	−0.010	−0.004	0.000	0.000	0.000	0.000
(100) (Cu)	0.667	0.661	0.663	0.680	0.643	0.469	−0.012	−0.004	0.000	0.000	0.000	0.000
(110) (Ni)	0.643	0.641	0.639	0.637	0.574	0.391	−0.004	−0.005	−0.001	−0.000	−0.000	0.000
(110) (Cu)	0.661	0.658	0.658	0.658	0.603	0.422	−0.007	−0.006	−0.001	−0.000	−0.000	0.000
(111) (Ni)	0.636	0.636	0.639	0.647	0.635	0.433	−0.011	−0.002	−0.001	0.000	0.000	−0.001
(111) (Cu)	0.647	0.647	0.651	0.660	0.651	0.463	−0.013	−0.002	−0.001	0.001	0.001	−0.001

$$\tilde{m}(r) = -\frac{1}{\pi}\int^{E_F} dE\, \mathrm{Im}[G_0^{\uparrow}(r,r,E) + \Delta G_L^{\uparrow}(r,r,E) + \Delta G_R^{\uparrow}(r,r,E) - G_0^{\downarrow}(r,r,E) - \Delta G_L^{\downarrow}(r,r,E) - \Delta G_R^{\downarrow}(r,r,E)], \quad (9)$$

which we can identify as

$$\tilde{m}(r) = m_L(r) + m_R(r) - m_0(r), \quad (10)$$

where $m_0(r)$ is the magnetization of the unperturbed spacer, i.e., the bulk spacer material. If we exclude multiple-scattering contributions, as well as possible magnetic enhancement/quenching effects, we may thus express the magnetic profile of the spacer material in a trilayer as a superposition of magnetization profiles of noninteracting free-standing bilayer interfaces. However, a major part of the enhancement/quenching effects are taken into account if the bilayer interfaces and surfaces are calculated self-consistently. Only parts of the enhancement/quenching effects due to multiple scattering and the superposition are not

TABLE II. The layer-resolved magnetic spin moments in units of Bohr magnetons of the Fe bcc, Co bcc, Co fcc, and Ni fcc surfaces calculated at the lattice constant determined by the corresponding experimental equilibrium volume. (vac. denotes vacuum.)

	$S-7$	$S-6$	$S-5$	$S-4$	$S-3$	$S-2$	$S-1$	S	$S+1$
Fe/vac. bcc									
(100) (Fe)	2.220	2.224	2.227	2.241	2.247	2.372	2.297	2.972	0.042
(110) (Fe)	2.237	2.236	2.228	2.222	2.221	2.250	2.346	2.572	0.014
(111) (Fe)	2.231	2.191	2.260	2.329	2.287	2.504	2.410	2.915	0.014
Co/vac. bcc									
(100) (Co)	1.732	1.735	1.730	1.735	1.739	1.741	1.711	1.938	−0.016
(110) (Co)	1.737	1.737	1.732	1.735	1.737	1.729	1.748	1.779	−0.023
(111) (Co)	1.743	1.728	1.743	1.743	1.735	1.727	1.778	2.005	−0.020
Co/vac. fcc									
(100) (Co)	1.654	1.653	1.653	1.655	1.645	1.663	1.633	1.840	−0.008
(110) (Co)	1.650	1.635	1.649	1.639	1.658	1.646	1.641	1.902	−0.009
(111) (Co)	1.638	1.639	1.638	1.638	1.640	1.633	1.672	1.721	−0.012
Ni/vac. fcc									
(100) (Ni)	0.649	0.650	0.653	0.652	0.642	0.660	0.642	0.694	−0.015
(110) (Ni)	0.647	0.628	0.656	0.640	0.637	0.649	0.646	0.766	−0.015
(111) (Ni)	0.636	0.637	0.636	0.632	0.635	0.648	0.677	0.622	−0.011

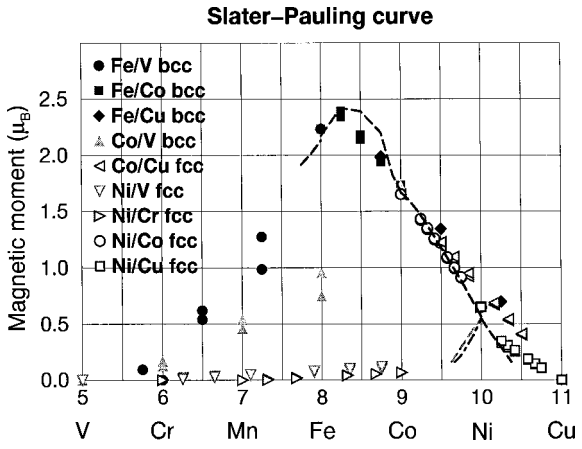

FIG. 2. The averaged interface moment $m_{AB}^{\mathrm{IF}}(\tilde{N})$, Eq. (1), as a function of valence charge $\tilde{N}$ for the different magnetic interfaces (Slater-Pauling curve). The dashed lines show the experimental moments for FeV, FeCo, CoNi, NiCu, and NiCr alloys. The dot-dashed line shows the moment for the NiV alloy.

accounted for. The superposition technique can directly be extended to include multilayer systems and superlattices since interlayer materials always are sandwiched between two neighboring materials, as in the case of a trilayer. Antiferromagnetically ordered multilayers are also easy to describe by superpositions, simply by changing sign of the magnetic moments of the corresponding magnetization profiles. Since the superposition formula, Eq. (10), also involves the spin moment of the unperturbed bulk material these are given in Table III for Fe, Co, and Ni.

In Figs. 3(a)–3(f) we display a few examples of the magnetization profiles in trilayers, calculated self-consistently and by means of the superposition formula, Eq. (10), with the magnetic moments taken from Tables I–III. As can be seen, multiple-scattering contributions or possible enhancement/quenching effects usually have a very small influence on the magnetic moments. Sometimes deviations between the self-consistent and superimposed magnetization profiles can be observed, for example, in Fig. 3(b). In this case a deep spin-dependent almost symmetric quantum well is surrounding the spacer material. Due to this quantum well there will be a relatively large difference in the multiple scattering of the majority and minority spin channels at the two interfaces. This is seen as a magnetic deviation between the two magnetization profiles, which actually may be viewed as a magnetic fingerprint of quantum-well states. However, the deviations are found to be small, almost constant shifts, and do not influence the shape of the magnetic profiles.[35]

TABLE III. The calculated magnetic bulk spin moments in units of Bohr magnetons of bcc Fe, bcc Co, fcc Co, and fcc Ni at different lattice constants. Each lattice constant is determined by the experimental atomic volumes of the material given within the parentheses.

	(V)	(Cr)	(Fe)	(Co)	(Ni)	(Cu)
Fe bcc	2.602		2.235	2.161		2.248
Co bcc	1.852		1.764	1.735		
Co fcc				1.653	1.641	1.682
Ni fcc	0.694	0.668		0.654	0.650	0.665

If the superposition is used to calculate the magnetic moment for single monolayers embedded between two semi-infinite crystals we may get large errors, especially for magnetic monolayers embedded in V and Cr. For example, with the superposition, Eq. (10), we may predict that a single monolayer of Ni fcc (111) embedded in V actually would get a moment of about $-0.6\mu_B$, but calculated self-consistently it is nonmagnetic. The explanation for this is not necessarily that multiple-scattering effects are large for single monolayers. If the interface magnetization in the bilayer is quenched due to the perturbation at the interface, the effect will be twice as large for the embedded monolayer. However, if we quench the magnetic moment twice we will not get back to the bulk moment, not even with an opposite sign. This phenomenon, which is of importance in case of embedded single monolayers of magnetic materials, is not accounted for in the superposition formula. The failure is due to the fact that the superposition formula was derived without taking all enhancement or quenching effects into account. Even if the single bilayer interfaces were calculated self-consistently, including enhancement or quenching effects, no such effects are taken into account after the superposition. An alternative way to estimate the magnetism of a single monolayer is instead to study the magnetization of the bulk alloy for a concentration corresponding to the coordination of the atoms in the embedded monolayer, analogous to what was discussed in the previous section.

VI. MAGNETIC CLUSTERS

Up till now only layered systems have been discussed. However, the superposition formula, Eq. (10), can be extended, not only to multilayers and superlattices, but also to objects where the symmetry is broken in more than one dimension. For example, six different planar magnetic interface perturbations are surrounding a cube of Ni embedded in fcc Cu. Interface perturbations, V_i $(i=1,2,\ldots,N)$, change the ground-state Green's function G_0^σ of the surrounded bulk material. The perturbed Green's function G^σ may be expressed according to Eq. (3) as

$$G^\sigma = G_0^\sigma + \sum_{i=1}^{N} \Delta G_i^\sigma + \Delta G_{QW}^\sigma, \tag{11}$$

where

$$\Delta G_i^\sigma = G_0^\sigma V_i^\sigma G_0^\sigma + G_0^\sigma V_i^\sigma G_0^\sigma V_i^\sigma G_0^\sigma + \cdots, \tag{12}$$

and

$$\Delta G_{QW}^\sigma = G_0^\sigma V_i^\sigma G_0^\sigma V_j^\sigma G_0^\sigma + \cdots \quad (i \neq j). \tag{13}$$

If multiple scattering in the quantum well formed between the different interface perturbations, i.e., ΔG_{QW}^σ, is neglected, we can, analogous to the previous discussion, describe the magnetic profile of the enclosed object $\tilde{m}(r)$ as a superposition of the magnetic profiles induced by the individual planar interfaces perturbations $m_i(r)$ as

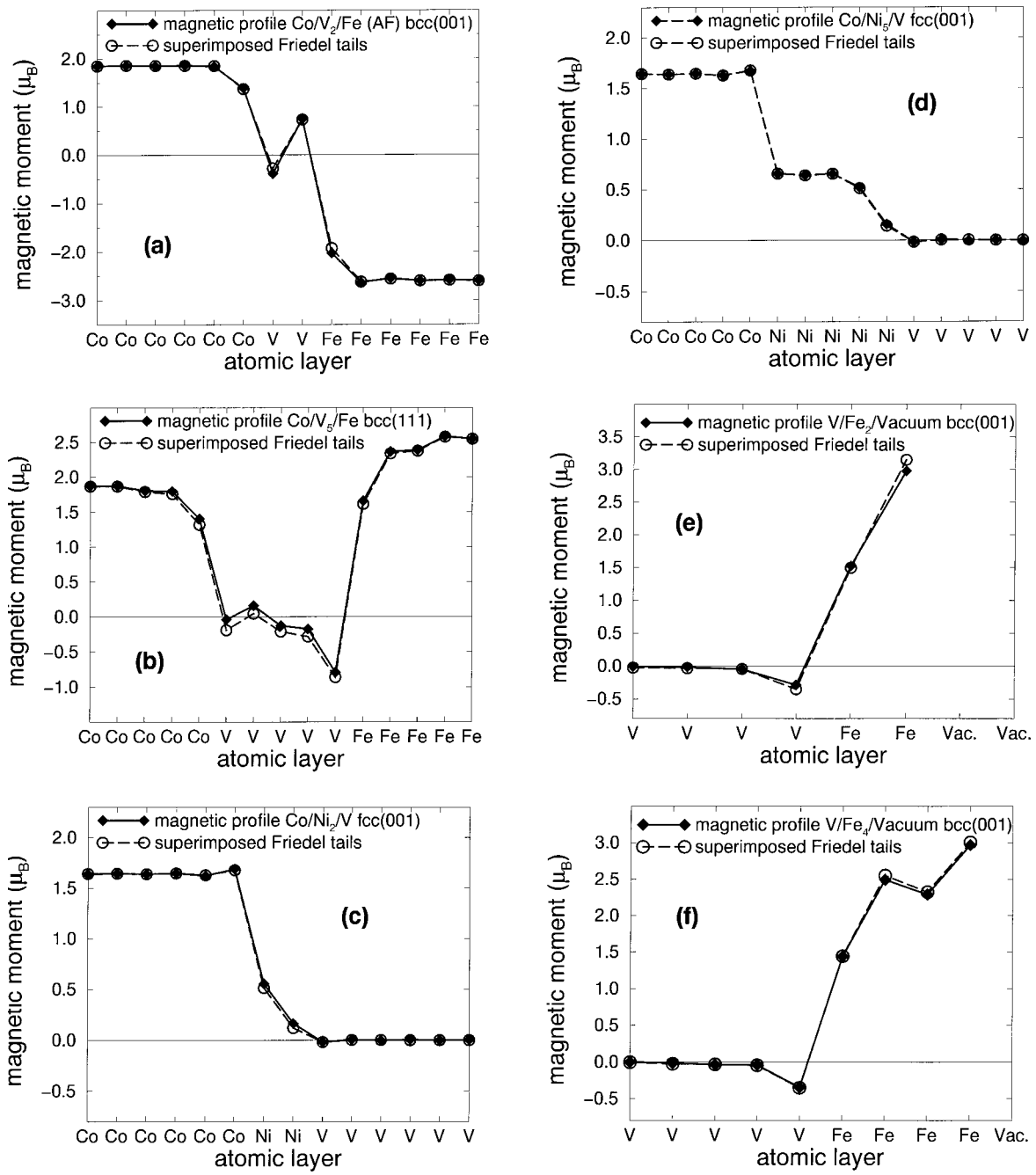

FIG. 3. The self-consistently calculated magnetic profiles of a few different layered systems [(a)–(f)] together with the magnetization derived from a superposition of the magnetic bilayer and surface profiles.

$$\tilde{m}(r)=\sum_{i=1}^{N} m_i(r)-(N-1)m_0(r). \tag{14}$$

Here $m_0(r)$ is the magnetization of the unperturbed enclosed material and N is the number of interface perturbations. By means of superposition of the tabulated magnetization (Tables I–III), we may now create the approximative magnetization profiles of any kind of objects demarcated by planar interfaces, such as atomic clusters or embedded magnetic polyhedrons. In the same way as we could use the trilayer superposition to construct the magnetization of more extended complex layered systems, we may equivalently use this more general superposition to estimate the magnetization of even more advanced objects, for example, the magnetization profile of a Fe bcc polyhedron placed on a Co bcc (110) surface. Relaxation effects will probably be much larger in these cases, but otherwise we have no reason to believe that the accuracy of such constructions should be less accurate than what was found in the case of the trilayers.

VII. SUMMARY

The layer-resolved magnetic spin moments of a number of 3*d* bilayer interfaces and surfaces have been calculated by means of a self-consistent density-functional method. We have shown how the magnetic profiles of the bilayers and

surfaces can be superimposed to construct the magnetic profiles of more complex magnetic systems. In this way we have obtained a very efficient technique to predict the approximate magnetization profile of almost any kind of system. The error of the superimposed magnetization profile, which essentially occurs due to multiple scattering between the interfaces, can be used to analyze the effect of spin-polarized QW states. Furthermore, the relation between the magnetic interface moments and the magnetization of the corresponding binary bulk alloy was investigated and it was shown how data from the bulk alloys could be used in order to estimate the interface magnetization. The explanation of the behavior of the interface magnetism can thus be traced back to the understanding of magnetism in bulk alloys.

ACKNOWLEDGMENT

Financial support from the Swedish Material Consortium No. 9 and NFR Grant No. 9871-321 are acknowledged.

[1] P. Grünberg, R. Schreiber, Y. Pang, M. B. Brodsky, and H. Sowers, Phys. Rev. Lett. **57**, 2442 (1986).
[2] S. S. P. Parkin, N. Moore, and K. P. Roche, Phys. Rev. Lett. **64**, 2304 (1990).
[3] S. S. P. Parkin, R. Bhadra, and K. P. Roche, Phys. Rev. Lett. **66**, 2152 (1991).
[4] H. Ebert, H. Winter, B. Gyorffy, D. D. Johnson, and F. J. Pinski, Solid State Commun. **64**, 1011 (1987).
[5] P. Hohenberg and W. Kohn, Phys. Rev. **136**, B864 (1964).
[6] W. Kohn and L. J. Sham, Phys. Rev. **140**, A1133 (1965).
[7] D. M. Ceperley and B. J. Alder, Phys. Rev. Lett. **45**, 566 (1980).
[8] S. H. Vosko, L. Wilk, and M. Nusair, Can. J. Phys. **58**, 1200 (1980).
[9] O. K. Andersen, Phys. Rev. B **12**, 3060 (1975).
[10] H. L. Skriver, *The LMTO Method* (Springer-Verlag, Berlin, 1984).
[11] O. K. Andersen and O. Jepsen, Phys. Rev. Lett. **53**, 2571 (1984).
[12] O. K. Andersen, O. Jepsen, and D. Glötzel, in *Highlights of Condensed-Matter Theory*, edited by F. Bassani, F. Fumi, and M. P. Tosi (North-Holland, New York, 1985).
[13] H. L. Skriver and N. M. Rosengaard, Phys. Rev. B **43**, 9538 (1991).
[14] P. O. Löwdin, J. Chem. Phys. **19**, 1396 (1951).
[15] B. Wenzien, J. Kudrnovsky, V. Drchal, and M. Sob, J. Phys.: Condens. Matter **1**, 9893 (1989).
[16] I. Turek, V. Drchal, J. Kudrnovsky, M. Sob, and P. Weinberger, *Electronic Structure of Disordered Alloys, Surfaces and Interfaces* (Kluwer Academic Publishers, Amsterdam, 1997).
[17] S. L. Cunningham, Phys. Rev. B **10**, 4988 (1973).
[18] P. James (private communication).
[19] M. Alde'n, S. Mirbt, H. L. Skriver, N. M. Rosengaard, and B. Johansson, Phys. Rev. B **46**, 6303 (1992).
[20] E. Wimmer, A. J. Freeman, and H. Krakauer, Phys. Rev. B **30**, 3113 (1984).
[21] O. Eriksson, G. W. Fernando, and R. C. Albers, Solid State Commun. **78**, 801 (1991).
[22] S. Ohnishi and A. J. Freeman, Phys. Rev. B **28**, 6741 (1983).
[23] C. Li and A. J. Freeman, J. Magn. Magn. Mater. **75**, 53 (1988).
[24] C. L. Fu and A. J. Freeman, J. Magn. Magn. Mater. **69**, L1 (1988).
[25] C. L. Fu and A. J. Freeman, J. Phys. (Paris), Colloq. **49**, C8-1625 (1988).
[26] M. Tischer, O. Hjortstam, D. Arvanitis, J. Hunter Dunn, F. May, K. Baberschke, J. Trygg, J. M. Wills, B. Johansson, and O. Eriksson, Phys. Rev. Lett. **75**, 1602 (1995).
[27] P. Srivastava, F. Wilhelm, A. Ney, M. Farle, H. Wende, N. Haack, G. Ceballos, and K. Baberschke, Phys. Rev. B **58**, 5701 (1998).
[28] B. Swinnen, J. Meersschaut, J. Dekoster, G. Langouche, S. Cottenier, S. Demuynck, and M. Rots, Phys. Rev. Lett. **78**, 362 (1997).
[29] B.-U. Runge, M. Dippel, G. Filleböck, K. Jacobs, U. Kohl, and G. Schatz, Phys. Rev. Lett. **79**, 3054 (1997).
[30] D. Bonnenberg, K. A. Hempel, and H. P. J. Wijn, in *Numerical Data and Functional Relationship in Science and Technology*, edited by K.-H. Hellwege and O. Madelung, Landolt-Börnstein, New Series, Group III, Vol. 19a (Springer-Verlag, Berlin, 1986), p. 142.
[31] P. James, O. Eriksson, B. Johansson, and I. A. Abrikosov, Phys. Rev. B **59**, 419 (1999).
[32] S. Å. Lindgren and L. Walldén, Phys. Rev. Lett. **59**, 3003 (1987).
[33] J. E. Ortega and F. J. Himpsel, Phys. Rev. Lett. **69**, 844 (1992).
[34] C. Carbone *et al.*, Phys. Rev. Lett. **71**, 2805 (1993).
[35] A. M. N. Niklasson, S. Mirbt, H. L. Skriver, and B. Johansson, Phys. Rev. B **53**, 8509 (1996).
[36] A. M. N. Niklasson, S. Mirbt, H. L. Skriver, and B. Johansson, Phys. Rev. B **56**, 3276 (1997).
[37] S. Mirbt, B. Johansson, and H. L. Skriver, Phys. Rev. B **53**, R13 310 (1996).